Published in final edited form as:
Nature. 2012 November 8; 491(7423): 254–258. doi:10.1038/nature11465.

Adenoma-linked barrier defects and microbial products drive IL-23/IL-17-mediated tumour growth

Sergei I. Grivennikov[1,*], **Kepeng Wang**[1,2,*], **Daniel Mucida**[3,4], **C. Andrew Stewart**[5], **Bernd Schnabl**[6], **Dominik Jauch**[1], **Koji Taniguchi**[1,7], **Guann-Yi Yu**[1], **Christoph H. Osterreicher**[6,8], **Kenneth E. Hung**[9], **Christian Datz**[10], **Ying Feng**[11], **Eric R. Fearon**[11], **Mohamed Oukka**[12], **Lino Tessarollo**[13], **Vincenzo Coppola**[14], **Felix Yarovinsky**[15], **Hilde Cheroutre**[3], **Lars Eckmann**[6], **Giorgio Trinchieri**[5], and **Michael Karin**[1]

[1]Laboratory of Gene Regulation and Signal Transduction, Departments of Pharmacology and Pathology, School of Medicine, University of California, San Diego, 9500 Gilman Drive, La Jolla, California 92093-0723, USA

[2]Biomedical Research Institute, Shenzhen-PKU-HKUST Medical Center, No. 1120, Lianhua Road, Shenzhen, Guangdong Province, China

[3]La Jolla Institute for Allergy and Immunology, La Jolla, California 92093, USA

[4]Laboratory of Mucosal Immunology, The Rockefeller University, New York, New York 10065, USA

[5]Cancer and Inflammation Program, Laboratory of Experimental Immunology, Center for Cancer Research, National Cancer Institute, National Institutes of Health, Frederick, Maryland 21702-1201, USA

[6]Department of Medicine, School of Medicine, University of California, San Diego, 9500 Gilman Drive, La Jolla, California 92093-0723, USA

[7]Department of Microbiology and Immunology, Keio University School of Medicine, Tokyo 160-8582, Japan

[8]Institute of Pharmacology, Center for Physiology and Pharmacology Medical University of Vienna, Vienna, Austria

[9]Department of Medicine, Tufts Medical Center, Boston, Massachusetts 02111, USA

[10]Department of Internal Medicine, Oberndorf Hospital, Paracelsus Medical University Salzburg, Austria

[11]Departments of Internal Medicine, Human Genetics and Pathology, University of Michigan Medical School, Ann Arbor, Michigan 48109, USA

[12]Seattle Children's Research Institute, Seattle, Washington 98105, USA

Correspondence and requests for materials should be addressed to M.K. (karinoffice@ucsd.edu).
*These authors contributed equally to this work.

Supplementary Information is available in the online version of the paper.

Author Contributions S.G. and M.K. conceived the project. S.G., K.W., D.M., B.S., D.J., K.T., G.Y.Y., C.O., Y.F. and K.E.H. performed the experiments. S.G., K.W., D.M., D.J., H.C., L.E. and M.K. analyzed data. C.A.S., V.C., L.T. and G.T. generated *Il23r*$^{F/F}$ mice. M.O. and F.Y. provided *Il23r*$^{gfp/gfp}$ and *Tlr2,4,9*$^{-/-}$ bone marrow, respectively, and Y.F. and E.R.F. provided CPC-APC mice and tissues from *Cdx2*$^{ERT\text{-}Cre}$-APC mice. C.A.S., E.R.F., H.C. and G.T. provided conceptual advice. C.D. collected and provided human specimens. S.G., K.W. and M.K. wrote the manuscript, with all authors contributing to the writing and providing advice.

The authors declare no competing financial interests. Readers are welcome to comment on the online version of the paper.

[13]Mouse Cancer Genetics Program, National Cancer Institute, National Institutes of Health, Frederick, Maryland 21702-1201, USA

[14]Department of Molecular Virology, Immunology & Medical Genetics, Ohio State University Comprehensive Cancer Center, Wexner Medical Center, Columbus, Ohio 43210, USA

[15]Department of Immunology, University of Texas Southwestern Medical Center at Dallas, Dallas, Texas 75390, USA

Abstract

Approximately 2% of colorectal cancer is linked to pre-existing inflammation known as colitis-associated cancer, but most develops in patients without underlying inflammatory bowel disease. Colorectal cancer often follows a genetic pathway whereby loss of the adenomatous polyposis coli (*APC*) tumour suppressor and activation of β-catenin are followed by mutations in *K-Ras*, *PIK3CA* and *TP53*, as the tumour emerges and progresses[1,2]. Curiously, however, 'inflammatory signature' genes characteristic of colitis-associated cancer are also upregulated in colorectal cancer[3,4]. Further, like most solid tumours, colorectal cancer exhibits immune/inflammatory infiltrates[5], referred to as 'tumour elicited inflammation'[6]. Although infiltrating $CD4^+$ T_H1 cells and $CD8^+$ cytotoxic T cells constitute a positive prognostic sign in colorectal cancer[7,8], myeloid cells and T-helper interleukin (IL)-17-producing (T_H17) cells promote tumorigenesis[5,6], and a 'T_H17 expression signature' in stage I/II colorectal cancer is associated with a drastic decrease in disease-free survival[9]. Despite its pathogenic importance, the mechanisms responsible for the appearance of tumour-elicited inflammation are poorly understood. Many epithelial cancers develop proximally to microbial communities, which are physically separated from immune cells by an epithelial barrier[10]. We investigated mechanisms responsible for tumour-elicited inflammation in a mouse model of colorectal tumorigenesis, which, like human colorectal cancer, exhibits upregulation of IL-23 and IL-17. Here we show that IL-23 signalling promotes tumour growth and progression, and development of a tumoural IL-17 response. IL-23 is mainly produced by tumour-associated myeloid cells that are likely to be activated by microbial products, which penetrate the tumours but not adjacent tissue. Both early and late colorectal neoplasms exhibit defective expression of several barrier proteins. We propose that barrier deterioration induced by colorectal-cancer-initiating genetic lesions results in adenoma invasion by microbial products that trigger tumour-elicited inflammation, which in turn drives tumour growth.

Specimens of human colorectal cancer (CRC) show increased expression of IL-23p19 and IL-17A messenger RNA (mRNAs) (Fig. 1a). IL-23p19 is the specific subunit of IL-23, a positive regulator of T_H17 and other IL-17-producing cells[11], previously found to promote skin carcinogenesis[12]. To address the role of these cytokines in CRC-related tumour-elicited inflammation and tumour growth, we used $Apc^{F/wt}$ mice that harboured a *Cdx2-Cre* transgene (CPC-APC mice) in which colorectal tumorigenesis was driven by *Apc* allelic loss[13]. Unlike Apc^{Min} mice, CPC-APC mice develop tumours primarily in the distal colon, providing a relevant model of human CRC[13]. Mouse colon tumours also exhibited marked upregulation of IL-23 and IL-17A mRNA and IL-23 protein relative to matched non-tumour colon (Fig. 1b, c). IL-23 induction was specific, as tumoural expression of other IL-12/23 family members was not substantially elevated and IL-23 itself was already seen in early tumours (Supplementary Fig. 1a, b). IL-23 expression did not further increase in more advanced mouse CRC caused by *Apc* loss and forced *K-Ras* or *B-Raf* activation (Supplementary Fig. 1c). Analysis of $Il23^{-/-}$ mice harbouring green fluorescent protein (GFP) gene in the *Il23p19* locus, staining with IL-23p19 antibody and flow cytometry showed that IL-23p19 is particularly expressed in tumour-infiltrating cells such as $CD11b^+$ and $F4/80^+$ myeloid cells (Supplementary Fig. 1d–f). Both IL-23 subunits, p19 and p40, need to be simultaneously expressed to generate a functional cytokine. Analysis by quantitative PCR with reverse transcription (RT-qPCR) and fluorescence-activated cell

sorting (FACS) of tumoural cell populations showed that $CD11b^+$ cells expressed substantial amounts of both p19 and p40 (Fig. 1d). T_H17- and other IL-17-producing cells were detected in mesenteric lymph nodes and tumours of CPC-APC mice and demonstrated dependence on IL-23 signalling (Fig. 1e). Thus, expression of IL-23 and its downstream target IL-17A is increased during spontaneous colorectal tumorigenesis.

Colorectal tumour multiplicity and growth were diminished upon ablation of IL-23 or IL-23R in CPC-APC mice (Fig. 1f, g and Supplementary Fig. 2a). Although intra-tumoural apoptosis was unaffected, cancer cell proliferation was reduced in *Il23*$^{-/-}$/CPC-APC mice (Supplementary Fig. 2b, c). Epithelial STAT3 phosphorylation was decreased without IL-23, but genetically driven nuclear β-catenin accumulation was unaffected (Fig. 1g and Supplementary Fig. 2d). IL-23 signalling was important for intra-tumoural production of downstream cytokines, which are either direct (IL-6, IL-22) or indirect (IL-17A) STAT3 activators (Fig. 1h). Pro-tumorigenic IL-23 signalling was particularly confined to the haematopoietic compartment, as CPC-APC chimaeras harbouring *Il23*$^{-/-}$or *Il23r*$^{gfp/gfp}$ bone marrow also exhibited reduced tumour load (Supplementary Fig. 3a–d) and diminished expression of IL-23-dependent cytokines (Supplementary Fig. 3e). To examine the role of IL-17 signalling in CRC tumorigenesis, we crossed CPC-APC mice with *Il17ra*$^{-/-}$ mice, which do not respond to either IL-17A or IL-17F. Both tumour multiplicity and growth were reduced in the absence of IL-17RA (Supplementary Fig. 4a–c).

We examined the cause of IL-23 upregulation in CRC. The commensal microflora regulates basal colonic IL-23 expression in naive mice[14]. Microbial products are sensed by Toll-like receptors (TLRs), which rely on the adaptors MyD88 and TRIF[15]. Similar to its effect on small intestinal polyps in *Apc*^{Min} mice[16], whole body MyD88 ablation reduced tumour multiplicity and growth in CPC-APC mice (data not shown). We transplanted *Myd88*$^{-/-}$, *Tlr2,4,9*$^{-/-}$ triple knockout or control bone marrow into lethally irradiated CPC-APC mice. Expression of IL-23p19 mRNA by sorted tumoural myeloid cells was decreased upon TLR/MyD88 inactivation in the haematopoietic compartment (Fig. 2a). Intratumoural expression of IL-6 and IL-17A was also dependent on MyD88 in bone-marrow-derived cells (Fig. 2b). Transplantation with *Myd88*$^{-/-}$or *Tlr2,4,9*$^{-/-}$ bone marrow reduced colorectal tumour growth (Fig. 2c and Supplementary Fig. 5). By contrast, deletion of IL-18R in bone marrow had no effect on tumorigenesis or IL-23 production by TAM (Supplementary Fig. 6a, b). Short-term depletion of intestinal microflora with a combination of broad spectrum antibiotics, which reduced microbial counts by over 99.9%, also inhibited IL-23 expression by TAM, resulting in reduced tumoural IL-17A and decreased STAT3 activation in cancer cells (Fig. 2d–f). Prolonged depletion of commensal microflora by antibiotic treatment for 3.5 months starting at weaning reduced tumour size and load in control CPC-APC mice but not in *Il23r*$^{-/-}$/CPC-APC counterparts (Fig. 2g), emphasizing the importance of microbial product-driven IL-23 signaling.

By injecting fluorescein isothyocyanate (FITC)-labelled dextran into clamped colonic loops, we found that tumour development in CPC-APC mice was associated with translocation of FITC-dextran into the circulation (Fig. 3a). This suggested that CRC development may result in increased penetration of microbial products or microbes into tumours. Indeed, Alexa488-labelled lipopolysaccharide (LPS) injected into colonic loops of CPC-APC mice translocated into tumours where it particularly co-localized with $F4/80^+$ TAMs, but did not penetrate adjacent normal tissue (Fig. 3b). Tumour development also coincided with elevated endotoxin in portal blood (Fig. 3c). Occasional bacteria were detected by *in situ* hybridization with a eubacterial 16S ribosomal RNA (rRNA) probe within colorectal tumours (Fig. 3d) and proximal to tumour epithelial cells in mouse early lesions that resembled aberrant crypt foci and early human adenomas (Fig. 3e, f).

Mucus from goblet cells prevents bacterial penetration through the colonic epithelial barrier. Correspondingly, *Muc2*$^{-/-}$ mice develop spontaneous colitis followed by colitis-associated cancer[17,18]. Periodic acid-Schiff staining indicated absence of mucus-producing cells and mucins in tumours but not in adjacent normal tissue (Fig. 4a). Staining with wheat germ agglutinin (WGA) for glycosylated mucus proteins and mucin 2 (Muc2)-specific antibody demonstrated markedly reduced Muc2 production and coating of tumour tissue (Fig. 4a). Muc2 was barely detected in human CRC, but was prominent in adjacent normal tissues (Fig. 4b). Muc2 mRNA was downregulated in human and mouse colorectal tumours relative to healthy tissues (Supplementary Fig. 7a, b). Epithelial barriers also depend on tight and adherent junctions[10]. Human CRC demonstrated notable loss of polarized expression of junctional proteins JAM-A and JAM-B (Fig. 4c). JAM-A/B mRNAs were also reduced in human CRC and JAM-C mRNA was downregulated in mouse tumours (Supplementary Fig. 7a, b) Although claudin 4 mRNA was not downregulated in human or mouse tumours (Supplementary Fig. 7a, b), the protein was no longer distinctly localized to tight junctions in human or mouse tumours, similar to claudins 3, 5 and 7 (Supplementary Fig. 8a, b). Early human adenomas also showed defective mucin expression and organization of tight junctions (Fig. 4d), coinciding with elevated IL-23 and IL-17A in adenoma tissue (Supplementary Fig. 9a). Early CRC lesions, such as aberrant crypt foci, are marked by enhanced expression and nuclear translocation of β-catenin, and such areas were devoid of WGA and JAM-A staining (Fig. 4e). To demonstrate further that barrier loss is an early and direct consequence of tumour emergence, we studied rapid colonic transformation in *Cdx2*$^{\text{ERT-Cre}}$ × *Apc*$^{\text{F/F}}$ mice using tamoxifen to induce bi-allelic APC inactivation. APC loss resulted in patches of proliferating transformed cells with enlarged nuclei, which coincided with loss of mucin and induction of IL-23 (Fig. 4f and Supplementary Fig. 9b).

Nearly all solid malignancies contain inflammatory infiltrates, influencing tumour promotion, progression and metastasis[5,6]. The contribution of inflammation to CRC pathogenesis is emphasized by the protective effect of non-steroidal anti-inflammatory drugs, such as aspirin[19], but sources of tumour-elicited inflammation in CRC were heretofore unknown. We now suggest that early CRC-inducing genetic events may cause local loss of barrier function and entry of microbial products into the tumour microenvironment. This results in activation of IL-23-producing myeloid cells, which regulate expression of downstream tumour-promoting cytokines, including IL-17 and IL-6. A similar mechanism may apply to other cancers that develop in epithelia that are exposed to commensal and pathogenic bacteria. Deregulation of tight junctions and cell–cell contacts was described in advanced human adenocarcinomas, but suggested to cause detachment of carcinoma cells from their neighbours, increased motility and metastasis[20]. The importance of the mucus layer is emphasized by whole body Muc2 deficiency, which causes colonic inflammation[17,18]. Prolonged treatment with dextran sulphate sodium, which promotes development of colitis-associated cancer in wild type (WT or *Apc*$^{\text{Min}}$ mice, also causes erosion of the intestinal epithelial barrier and microbial-dependent inflammation[21,22], and so do the barrier-disrupting pathogens *Citrobacter rodentium*[23] and enterotoxic *Bacteroides fragilis*[24]. The commensal microflora was suggested to promote adenoma development, as germ-free *Apc*$^{\text{Min}}$ mice exhibit a twofold reduction in small intestinal adenomas[25] and *Tbx21*$^{-/-}$;*Rag2*$^{-/-}$ulcerative colitis (TRUC) and *Il10*$^{-/-}$ mice fail to develop colitis-associated cancer when rendered germ-free[26,27]. Our work demonstrates that defective expression of barrier proteins is an early event in CRC tumorigenesis, coupled to upregulation of IL-23 and its downstream cytokines. We also found that IL-23 does not act directly on adenoma cells and that its receptor is expressed and signals within the haematopoietic compartment. Probably, IL-23 acts through IL-17 family members, as ablation of IL-17R attenuated colorectal tumorigenesis. IL-23 is instrumental for stabilizing the 'T_H17 signature', which includes IL-17A, RORγt and IL-23R, and was linked to extremely poor prognosis in human stage I/II CRC, which otherwise show 75–90%

survival[9]. IL-23 itself is not a part of the 'T_H17 signature', arguably because its expression is already elevated in early colorectal tumours. The 'IL-23/T_H17' and 'T_H1-cytotoxic' signatures are not mutually exclusive in human CRC[9]. Although in genetically uniform mice in barrier facilities IL-23 invariably leads to IL-17 induction, the genetic heterogeneity of human populations and their exposure to a broader spectrum of microbes may explain why certain individuals mount a stronger T_H17 response than others. T_H17 development is promoted by several cytokines, including IL-21, IL-6 and IL-1, all of which can be induced by microbial components[28]. It remains to be investigated which of these cytokines contributes to the tumoural T_H17 response and how it is affected by distinct microflora components. Segmented filamentious bacteria persisting in proximity to epithelial cells initiate T_H17 responses in the small intestine[29]. In tumours lacking protective barrier, other microbial species and products may invade the tumour and influence the 'IL-23/T_H17' signature.

Loss of APC and activation of β-catenin induces a proliferative state and blocks the differentiation of certain IEC lineages, including mucin-producing goblet cells[30]. Epithelial barrier loss may therefore be a consequence of β-catenin activation and/or of APC loss, which apart from β-catenin can also control cytoskeleton dynamics. Hence, early barrier loss and activation of IL-23/IL-17-driven tumour-elicited inflammation act additively and sequentially to genetically controlled events that govern CRC development and progression (Supplementary Fig. 10). We propose that screening of early tumours for IL-17 expression and adjuvant treatment of patients showing a 'T_H17 signature' with IL-23 or IL-17 antagonists should reduce mortality due to CRC.

METHODS

Human samples

Paraffin-embedded human ulcerative colitis and CRC specimens were provided by Oberndorf Hospital, Paracelsus Medical University Salzburg, Austria. Patients with ulcerative colitis or sporadic CRC underwent colonoscopy as a part of the diagnostic workup at the Department of Internal Medicine, Oberndorf Hospital (Salzburg, Austria). Diagnosis of ulcerative colitis was based on appropriate clinical, endoscopic, histopathological and radiological findings that satisfied the internationally accepted Lennard-Jones criteria[31]. Additionally, colonoscopic findings were classified as tubular adenoma, size less than 6 mm (early lesion), advanced adenoma (that is, villous or tubulovillous features), size at least 1 cm or high-grade dysplasia or carcinoma after a combined analysis of macroscopic and histological results[32,33]. Biopsies from colonic tissue with macroscopically normal appearance were taken in patients who underwent colonoscopy for CRC screening. For histological examination, specimens were fixed in 4% buffered formalin and embedded into paraffin. When available, a small tissue portion of the biopsy specimen was separated and preserved for RNA and protein extraction in RNA later (Ambion's RNA later solution, Applera, Brunn am Gebirge, Austria). Biopsies from colonic tissue with macroscopically normal appearance were taken in patients who underwent colonoscopy for CRC screening. Written informed consent was obtained from all study participants to use one biopsy specimen for scientific purposes. The study was approved by the local ethics committee (Ethikommission des Landes Salzburg, approval number 415-E/1262/2–2010). Frozen human CRC and normal colon tissues were obtained from Cooperative Human Tissue Network of Vanderbilt University Medical Center.

Generation of *Il23r*$^{F/F}$ and *Il23r*$^{-/-}$ mice

The targeted region includes exons 2 (3,708–3,810) and 3 (8,085–8,381) of *Il23r* that encode a portion of the signal peptide and the amino (N)-terminal Ig-like domain (Supplementary

Fig. 11a). The targeting vector was generated by recombineering using λ phage *Red* as described by Liu *et al.*[34]. Homology arms for the retrieval vector were amplified by PCR on C57BL/6 genomic DNA. Homology arms were cloned into pLMJ235 (pBSKS+ containing a 2.8kb SalI TK fragment of pGKTK) by triple ligation to form the retrieval plasmid. Retrieval of the targeting region (covering 753–12,812; numbering relative to indicated BamHI site) was performed according to Liu *et al.*[34] using C57BL/6 bacterial artificial chromosome RP23-283M8 (BACPAC Resources) as template in DY380 cells. Recombineering was performed to insert cassettes containing *LoxP*-flanked Neo cassettes from pGKEM7Neo-pA into the targeting vector. First, *LoxP-Neo-loxP* was inserted at position 3,524, followed by induced expression of *Cre* in EL350 cells to excise the *Neo* selection cassette but leaving the upstream *LoxP* site. A second cassette (*LoxP-Frt-Intron-Eng2SA-Neo-LoxP-Frt*) was inserted into position 8,503. After NotI-linearization, the targeting construct was electroporated into Bruce 4 C57BL/6 ES cells, and G418-selected clones were screened for integration by Southern analysis using sequences outside the targeting vector (Supplementary Fig. 11b). Selected clones were injected into C57BL/6-albino blastocysts and transferred to pseudopregnant females. Chimeric offspring were bred with C57BL/6-Albino partners to generate F_1 mice that were screened for integration by Southern blotting (Supplementary Fig. 11c). Resulting mice with the $Il23r^{SA\text{-}F\text{-}neo}$ allele were crossed with C57BL/6-FLPe mice to facilitate recombination between *Frt* sequences and generate the $Il23r^{F}$ allele. The null allele ($Il123r^{-/-}$) was generated by crossing $Il23r^{F/F}$ mice with *CPC-Cre* transgenic mice. The F_2 generation exhibits germline deletion of floxed alleles owing to early *CPC-Cre* expression in caudal regions of the body and gonads[13]. Complete ablation of IL-23R was confirmed by RT–qPCR of spleen and tumour-derived cells.

Animal models

C57Bl/6 control mice obtained from Charles River Laboratories were bred locally at University of California, San Diego. $Il23^{-/-}$ and $Il17ra^{-/-}$ mice were from Genentech[35] and Amgen[36], respectively. Bone marrow from $Il23r^{gfp/gfp}$ and $Tlr2,4,9^{-/-}$ mice was provided by M. Oukka[37] and F. Yarovinsky[38], respectively. $Apc^{F/F}$ and *Cdx2-Cre* (*CPC-Cre*) mice[13] were provided by E. Fearon, who also generated the $Cdx2\text{-}Cre^{ERT}$ mice, which will be described elsewhere. $Myd88^{-/-}$ mice[39] were obtained from the Jackson Laboratory, and $Il18r^{-/-}$ mice[40] were from H. Hoffman. All mice were maintained in filter-topped cages on autoclaved food and water at University of California, San Diego, according to NIH guidelines, and all experiments were performed in accordance with University of California, San Diego, and NIH guidelines and regulations. Most experiments used littermate controls housed in the same cage; in addition, dirty beddings were switched between cages of the same experiment to make sure that the microflora was balanced.

For spontaneous CRC tumorigenesis, male and female CPC-APC mice were allowed to develop colorectal tumours spontaneously for 4–5 months and then killed. Macroscopic tumours were counted and their diameter measured with a calliper. Average tumour size per individual mouse was determined by averaging diameters of all tumours present. Tumour load was determined as the sum of the diameters of all tumours presented in a given mouse, as previously described[41]. Typically, one-half of the distal colon was taken as a tissue sample, tumours and normal tissue dissected and snap-frozen in liquid nitrogen or used for *ex vivo* cultures or fluorescence-activated cell sorting. The other half was fixed in 10% neutral buffered formalin for 24 h and transferred to 70% ethanol for subsequent paraffin embedding, or alternatively frozen in optimal cutting temperature (O.C.T.) compound for further sectioning and histological analysis.

To induce colorectal tumours with inactivated *Apc* and activated *K-Ras* or *B-Raf*, open laparotomies were performed in mice bearing floxed *Apc* ($Apc^{F/F}$) in combination with

either latent $Kras^{G12D}$ (*Apc-Kras*) or $Braf^{V600E}$ (*Apc-Braf*) alleles under isofluorane anaesthesia. A dosage of adenovirus-Cre was administered to the distal colon, which resulted in solitary colonic tumours, as described[42,43]. Subsequent tumour formation was monitored by serial optical colonoscopy. Tumours were collected after more than 75% occlusion of the colonic lumen was observed and banked in RNA later for subsequent analysis.

Colonic loops and injections of FITC-dextran and Alexa488-LPS

After anaesthesia, a midline laparotomy incision was made. A 2–3 cm long segment of the colon with or without tumours inside was created with two vascular haemoclips without disrupting the mesenteric vascular arcades. The length of intestine between the two clips was injected with 50μl of 100 mg ml^{-1} FITC-dextran solution or 50μl of Alexa488-LPS at 70μg per mouse. At the indicated time points, mice were sacrificed and fluorescence was measured in the plasma with a fluorimeter, or colon fragments were embedded into O.C.T. compound, and frozen sections prepared and analysed for Alexa488-LPS tissue distribution by fluorescent microscopy.

Antibiotic treatment

Mice were given the following antibiotics in their drinking water: 100μg ml^{-1} neomycin, 50μg ml^{-1} vancomycin, 50μg ml^{-1} imipenem, 100μg ml^{-1} metronidazole, 50μg ml^{-1} streptomycin and 100 U ml^{-1} penicillin. Fresh antibiotics were supplied every week. For long-term antibiotic treatment after 2 months of initial treatment, drinking water was further supplemented with streptomycin (1 mg ml^{-1}), gentamycin (170μg ml^{-1}), ciprofloxacin (125μg ml^{-1}) and bacitracin 1 mg ml^{-1} as previously described[44]. Control mice were placed on bottled water. Faeces were collected and cultured on 5% sheep blood agar plates (Fisher Scientific) under aerobic or anaerobic conditions at 37 °C to determine the extent of colon sterilization, which exceeded 99.9%. Alternatively, DNA was isolated from stools of mice using QIAamp DNA Stool mini kit (Qiagen) and content of 16S bacterial rRNA was analysed by RT–qPCR. Mice were kept on antibiotics for the indicated time and sacrificed for tumour and tissue analysis.

Portal blood vein drainage and endotoxin measurement

Mice were anaesthetized with isofluorane and their portal vein exposed to insert a 28-gauge needle and draw 100–200μl of blood, which was collected into EDTA coated tubes (BD Biosciences). Plasma was isolated by centrifugation and endotoxin amounts were determined by microplate Limulus Amebocyte Lysate (LAL) colorimetric bioassay (Lonza) according to the manufacturer's recommendations.

Bone marrow transplantation

Six- to eight-week-old littermate recipient mice were irradiated twice during one day to achieve a lethal dose (2 × 600 rad) and intravenously injected with single cell suspension containing 10^7 donor bone marrow cells. Every cage of recipient mice contained mice receiving both gene-deficient and wild-type bone marrow to compare mice living in the same cage. For 2 weeks after irradiation, mice were placed on sulphamethoxazole and trimethoprime antibiotics in drinking water followed by transfer to the cages from the same room/rack with dirty bedding to restore microflora. Mice were killed and analysed for tumour development 4–5 months after transplantation.

Antibodies and stains

Fluorescent-labelled antibodies for flow cytometry were from eBioscience. Immunoblot analysis and immunohistochemistry were performed with antibodies to Ki-67, claudin7,

claudin 5, claudin 4, claudin 3, JAM-B, mucin2, GFP, IL-23p19 (Genetex), JAM-A (Santa Cruz), active caspase 3, phospho-STAT3 (Cell Signaling), F4/80 and E-cadherin (BD Biosciences). Secondary antibodies (host: donkey) for fluorescent microscopy labelled with Alexa 488 or 594 were from Invitrogen. For TdT-mediated dUTP nick end labelling (TUNEL) assay the *In situ* Cell Death Kit (Roche) was used according to the manufacturer's recommendations. Alexa488-LPS and Oregon488-WGA were from Invitrogen.

Immunohistology

Paraffin-embedded slides were de-paraffinized. Antigen unmasking was performed by incubation in 94 °C water bath in 10 mM sodium citrate buffer with 0.1% Tween 20 for 1 hour. Slides were incubated with primary antibodies in PBS containing 1% BSA and 10% normal goat or donkey serum, depending on the host of secondary antibodies used. Biotinylated secondary anti-rat or anti-rabbit antibodies (Pharmingen) were added and incubated at room temperature for 1 h. Streptavidin-HRP (Pharmingen) was added and after 40 min the sections were developed with DAB substrate and counterstained with haematoxylin. Alternatively, paraffin-embedded or acetone fixed frozen slides were stained with antibodies followed by secondary donkey antibodies labelled with Alexa 488 or Alexa 594, counterstained with DAPI and analysed by immunofluorescence. Images were acquired on an upright light/fluorescent Imager A2 microcope (Zeiss) equipped with an AxioCam camera or on a confocal microscope (Leica SPE).

Bacteria fluorescent *in situ* hybridization

Paraffin embedded slides were de-paraffinized and hybridized to universal eubacterial or control probes labelled with Alexa-594. Hybridization was performed in 48 °C oven for 2 h followed by washing and counter-stained by DAPI. The sequences of the probes are listed below: Eubacteria: GCTGCCTCCCGTAGGAGT; control: CGACGGAGGGCATCCTCA.

Flow cytometry and cell sorting

Isolated cells were stained with labelled antibodies in PBS with 2% FCS and analysed on a BD LSRII or on an Accuri C6 flow cytometer. Dead cells were excluded on the basis of staining with Live/Dead fixable Aqua dye (Invitrogen). For intracellular cytokine staining cell were restimulated in the presence of Brefeldin A as indicated, fixed and permeabilized with Cytofix/Cytoperm reagent (BD Biosciences) according to the manufacturer's recommendations and stained with labelled antibody for the cytokine of interest. For cell sorting, a BD FACSAria II cell sorter was used. Data were analysed using FlowJo software (Treestar).

ELISA

Pieces (20–40 mg) of normal or tumour tissue were cultured in 0.5 ml RPMI medium supplemented with antibiotics and 2% FCS at 37 °C for 24 h. Supernatants were collected, centrifuged and concentration of IL-23 protein was determined using ELISA Quantikine kit (R&D Systems) according to the manufacturer's recommendations.

RT–qPCR analysis

Total RNA was extracted using RN easy Plus kit to eliminate genomic DNA contamination (Qiagen). RNA was reverse transcribed using a IScript kit (Biorad). RT–qPCR was performed using EvaGreen PCR mix (Biorad) on a Biorad CFX96 machine. Expression data were normalized to L32 mRNA expression. The data are presented in arbitrary units and were calculated as $2^{(Ct(rpl32-gene\ of\ interest))}$. Primer sequences are listed in Supplementary Table 1 and generally were obtained from the NIH qPrimer Depot for mouse (http://mouseprimerdepot.nci.nih.gov) and human (http://primerdepot.nci.nih.gov). Whenever

possible, primers were intron-spanning, such that amplification was only feasible on complementary DNA.

Statistical analysis

Data are presented as averages ± s.e.m. and were analysed by built-in *t*-test using Microsoft Excel software. *P* values less than 0.05 were considered significant.

Supplementary Material

Refer to Web version on PubMed Central for supplementary material.

Acknowledgments

We thank eBioscience, GeneTex, Santa Cruz, BioLegend and Cell Signaling for antibodies; Genentech and Amgen for *Il23*$^{-/-}$ and *Il17ra*$^{-/-}$ mice, respectively, and S. Reid and E. Southon for the help in generating *Il23r*$^{F/F}$ mice. This work was supported by Crohn's and Colitis Foundation of America (career development award number 2693), NIH/National Institute of Diabetes and Digestive and Kidney Diseases (K99-DK088589) and a University of California, San Diego, Digestive Disease Research Development Center Pilot Grant (DK080506) to S.G.; Croucher Foundation and China Postdoctoral Science Foundation (20110490919) to K.W.; Strategic Young Researcher Overseas Visits Program for Accelerating Brain Circulation to K.T.; SPAR Austria to C.D.; NIH (R01CA082223) to E.R.F.; and NIH (AI043477; DK035108) and American Association for Cancer Research (07-60-21-KARI) grants to M.K., who is an American Cancer Society Research Professor. The content is solely the responsibility of the authors and does not necessarily represent the official views of the NIH.

References

1. Vogelstein B, Kinzler KW. Cancer genes and the pathways they control. Nature Med. 2004; 10:789–799. [PubMed: 15286780]
2. Fearon ER, Vogelstein B. A genetic model for colorectal tumorigenesis. Cell. 1990; 61:759–767. [PubMed: 2188735]
3. Wood LD, et al. The genomic landscapes of human breast and colorectal cancers. Science. 2007; 318:1108–1113. [PubMed: 17932254]
4. Reichling T, et al. Transcriptional profiles of intestinal tumors in Apc(Min) mice are unique from those of embryonic intestine and identify novel gene targets dysregulated in human colorectal tumors. Cancer Res. 2005; 65:166–176. [PubMed: 15665292]
5. Mantovani A, Allavena P, Sica A, Balkwill F. Cancer-related inflammation. Nature. 2008; 454:436–444. [PubMed: 18650914]
6. Grivennikov SI, Greten FR, Karin M. Immunity, inflammation, and cancer. Cell. 2010; 140:883–899. [PubMed: 20303878]
7. Schreiber RD, Old LJ, Smyth MJ. Cancer immunoediting: integrating immunity's roles in cancer suppression and promotion. Science. 2011; 331:1565–1570. [PubMed: 21436444]
8. Galon J, et al. Type, density, and location of immune cells within human colorectal tumors predict clinical outcome. Science. 2006; 313:1960–1964. [PubMed: 17008531]
9. Tosolini M, et al. Clinical impact of different classes of infiltrating T cytotoxic and helper cells (Th1, th2, treg, th17) in patients with colorectal cancer. Cancer Res. 2011; 71:1263–1271. [PubMed: 21303976]
10. Brenchley JM, Douek DC. Microbial translocation across the GI tract. Annu Rev Immunol. 2012; 30:149–173. [PubMed: 22224779]
11. McKenzie BS, Kastelein RA, Cua DJ. Understanding the IL-23-IL-17 immune pathway. Trends Immunol. 2006; 27:17–23. [PubMed: 16290228]
12. Langowski JL, et al. IL-23 promotes tumour incidence and growth. Nature. 2006; 442:461–465. [PubMed: 16688182]
13. Hinoi T, et al. Mouse model of colonic adenoma-carcinoma progression based on somatic Apc inactivation. Cancer Res. 2007; 67:9721–9730. [PubMed: 17942902]

14. Sawa S, et al. RORγt^{+} innate lymphoid cells regulate intestinal homeostasis by integrating negative signals from the symbiotic microbiota. Nature Immunol. 2011; 12:320–326. [PubMed: 21336274]
15. Medzhitov R. Recognition of microorganisms and activation of the immune response. Nature. 2007; 449:819–826. [PubMed: 17943118]
16. Rakoff-Nahoum S, Medzhitov R. Regulation of spontaneous intestinal tumorigenesis through the adaptor protein MyD88. Science. 2007; 317:124–127. [PubMed: 17615359]
17. Van der Sluis M, et al. Muc2-deficient mice spontaneously develop colitis, indicating that MUC2 is critical for colonic protection. Gastroenterology. 2006; 131:117–129. [PubMed: 16831596]
18. Velcich A, et al. Colorectal cancer in mice genetically deficient in the mucin Muc2. Science. 2002; 295:1726–1729. [PubMed: 11872843]
19. Rothwell PM, et al. Effect of daily aspirin on long-term risk of death due to cancer: analysis of individual patient data from randomised trials. Lancet. 2011; 377:31–41. [PubMed: 21144578]
20. Wang X, Tully O, Ngo B, Zitin M, Mullin JM. Epithelial tight junctional changes in colorectal cancer tissues. Sci World J. 2011; 11:826–841.
21. Tanaka T, et al. Dextran sodium sulfate strongly promotes colorectal carcinogenesis in Apc(Min/+) mice: inflammatory stimuli by dextran sodium sulfate results in development of multiple colonic neoplasms. Int J Cancer. 2006; 118:25–34. [PubMed: 16049979]
22. Meira LB, et al. DNA damage induced by chronic inflammation contributes to colon carcinogenesis in mice. J Clin Invest. 2008; 118:2516–2525. [PubMed: 18521188]
23. Newman JV, Kosaka T, Sheppard BJ, Fox JG, Schauer DB. Bacterial infection promotes colon tumorigenesis in Apc(Min/+) mice. J Infect Dis. 2001; 184:227–230. [PubMed: 11424022]
24. Wu S, et al. A human colonic commensal promotes colon tumorigenesis via activation of T helper type 17 T cell responses. Nature Med. 2009; 15:1016–1022. [PubMed: 19701202]
25. Dove WF, et al. Intestinal neoplasia in the ApcMin mouse: independence from the microbial and natural killer (beige locus) status. Cancer Res. 1997; 57:812–814. [PubMed: 9041176]
26. Yang L, Pei Z. Bacteria, inflammation, and colon cancer. World J Gastroenterol. 2006; 12:6741–6746. [PubMed: 17106919]
27. Garrett WS, et al. Colitis-associated colorectal cancer driven by T-bet deficiency in dendritic cells. Cancer Cell. 2009; 16:208–219. [PubMed: 19732721]
28. Zhou L, et al. IL-6 programs T(H)-17 cell differentiation by promoting sequential engagement of the IL-21 and IL-23 pathways. Nature Immunol. 2007; 8:967–974. [PubMed: 17581537]
29. Ivanov II, et al. Specific microbiota direct the differentiation of IL-17-producing T-helper cells in the mucosa of the small intestine. Cell Host Microbe. 2008; 4:337–349. [PubMed: 18854238]
30. Barker N, et al. Crypt stem cells as the cells-of-origin of intestinal cancer. Nature. 2009; 457:608–611. [PubMed: 19092804]
31. Lennard-Jones JE. Classification of inflammatory bowel disease. Scand J Gastroenterol Suppl. 1989; 170:2–6. [PubMed: 2617184]
32. Bond JH. Polyp guideline: diagnosis, treatment, and surveillance for patients with colorectal polyps. Practice Parameters Committee of the American College of Gastroenterology. Am J Gastroenterol. 2000; 95:3053–3063. [PubMed: 11095318]
33. Winawer SJ, Zauber AG. The advanced adenoma as the primary target of screening. Gastrointest Endosc Clin N Am. 2002; 12:1–9. [PubMed: 11916153]
34. Liu P, Jenkins NA, Copeland NG. A highly efficient recombineering-based method for generating conditional knockout mutations. Genome Res. 2003; 13:476–484. [PubMed: 12618378]
35. Ghilardi N, et al. Compromised humoral and delayed-type hypersensitivity responses in IL-23-deficient mice. J Immunol. 2004; 172:2827–2833. [PubMed: 14978083]
36. Ye P, et al. Requirement of interleukin 17 receptor signaling for lung CXC chemokine and granulocyte colony-stimulating factor expression, neutrophil recruitment, and host defense. J Exp Med. 2001; 194:519–527. [PubMed: 11514607]
37. Awasthi A, et al. Cutting edge: IL-23 receptor gfp reporter mice reveal distinct populations of IL-17-producing cells. J Immunol. 2009; 182:5904–5908. [PubMed: 19414740]

38. Kirkland D, et al. B cell-intrinsic MyD88 signaling prevents the lethal dissemination of commensal bacteria during colonic damage. Immunity. 2012; 36:228–238. [PubMed: 22306056]

39. Kawai T, Adachi O, Ogawa T, Takeda K, Akira S. Unresponsiveness of MyD88-deficient mice to endotoxin. Immunity. 1999; 11:115–122. [PubMed: 10435584]

40. Hoshino K, et al. Cutting edge: generation of IL-18 receptor-deficient mice: evidence for IL-1 receptor-related protein as an essential IL-18 binding receptor. J Immunol. 1999; 162:5041–5044. [PubMed: 10227969]

41. Grivennikov S, et al. IL-6 and Stat3 are required for survival of intestinal epithelial cells and development of colitis-associated cancer. Cancer Cell. 2009; 15:103–113. [PubMed: 19185845]

42. Kim P, et al. In vivo wide-area cellular imaging by side-view endomicroscopy. Nature Methods. 2010; 7:303–305. [PubMed: 20228814]

43. Hung KE, et al. Development of a mouse model for sporadic and metastatic colon tumors and its use in assessing drug treatment. Proc Natl Acad Sci USA. 2010; 107:1565–1570. [PubMed: 20080688]

44. Chen GY, Shaw MH, Redondo G, Nunez G. The innate immune receptor Nod1 protects the intestine from inflammation-induced tumorigenesis. Cancer Res. 2008; 68:10060–10067. [PubMed: 19074871]

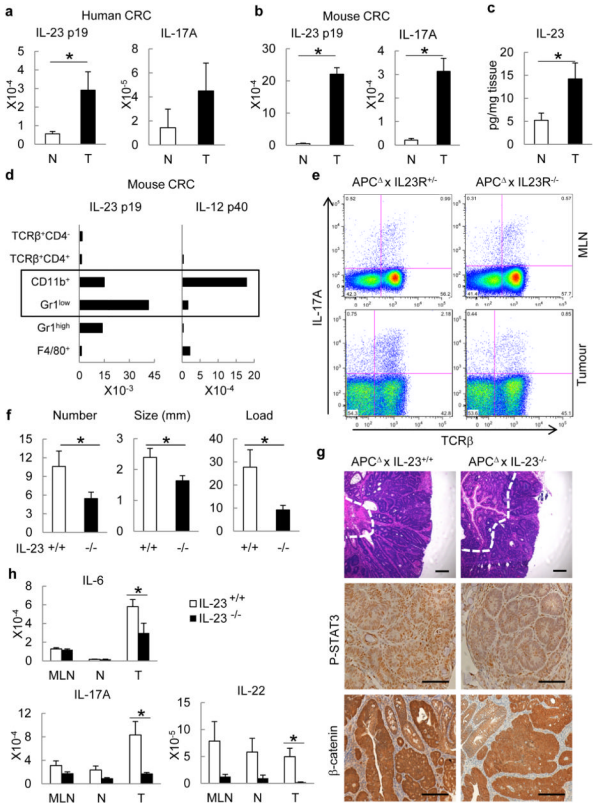

Figure 1. IL-23 controls CRC inflammation and tumorigenesis

a, **b**, RT–qPCR for IL-23p19 and IL-17A mRNAs from colorectal tumours (T) and matching normal (N) colons of (**a**) human CRC patients ($n = 7$, $P = 0.037$ for IL-23p19) or (**b**) CPC-APC mice ($n = 8$, $P = 5 \times 10^{-5}$, 3.6×10^{-4}, respectively). **c**, IL-23 protein was measured by ELISA in supernatants of cultured tumours and normal tissues of CPC-APC mice ($n = 5$, $P = 0.04$). **d**, RT–qPCR analysis of sorted haematopoietic myeloid cells ($CD45^+TCR\beta^-$ $CD11b^+$) from tumours of CPC-APC mice ($n = 4$; pooled); populations: $CD11b^+ = Gr1^-F4/80^{low}$; $Gr1^+ = Gr1^+F4/80^-$ $Gr1^{high} = Gr1^{high}F4/80^-$ $F4/80^+ = Gr1^{-/dim}F4/80^+$ and T cells ($CD45^+TCR\beta^+$). **e**, Intracellular cytokine staining of phorbol myristate acetate and ionomycin re-stimulated cells (Live/$Dead^-CD45^+$ gate). **f**, Five-month-old *Il23*$^{-/-}$ and control CPC-APC mice were sacrificed and tumour numbers, size and load were determined ($n = 7$, $P = 0.04$, 0.03, 0.01, respectively). **g**, Tumour sections were stained with haematoxylin and eosin or phospho-STAT3 and β-catenin antibodies. **h**, Cytokine mRNA analysis by RT–qPCR in mesenteric lymph nodes (MLN), normal (N) and tumour (T) tissue of 5-month-old *Il23*$^{-/-}$ and control CPC-APC mice ($n = 6$, $P = 0.044$, 0.007, 0.045, respectively). Data represent averages ± s.e.m. $^*P < 0.05$. Scale bars, 100μm.

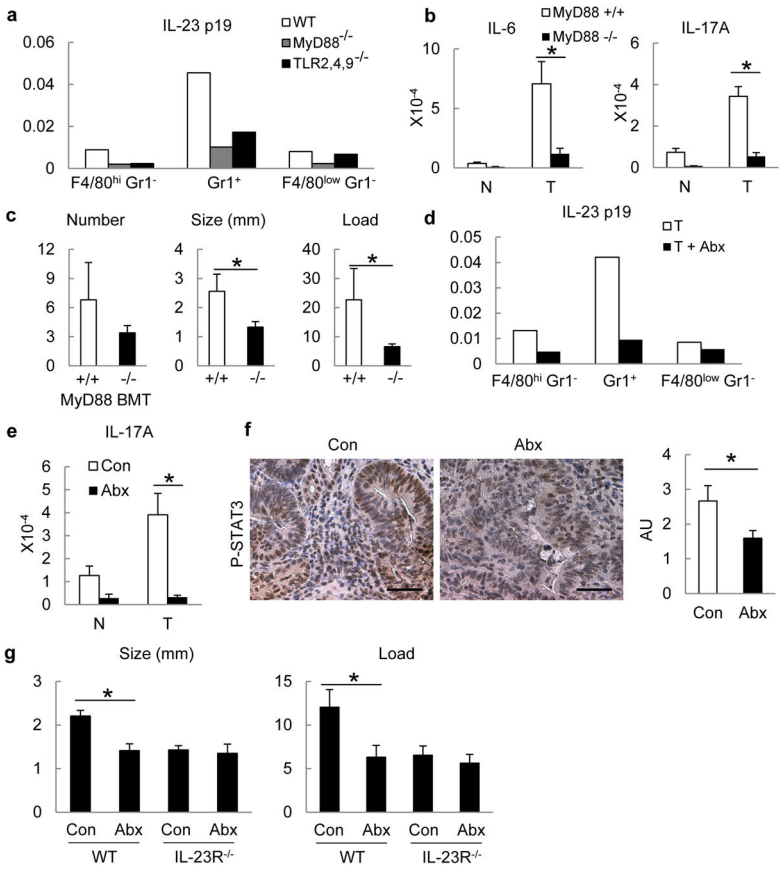

Figure 2. TLR-MyD88 signalling and commensal microflora promote cytokine expression and tumorigenesis

a–**c**, CPC-APC mice were transplanted with *Myd88*$^{-/-}$, *Tlr2,4,9*$^{-/-}$ or control bone marrow (BM)and analysed 4 months later by RT–qPCR for cytokine mRNAs in sorted tumour myeloid cells (Live/Dead^{-} TCRβ^{-} CD11b^{+}), representative of two independent experiments, each including four pooled mice (**a**) or in tumours and normal tissues ($n = 5$, $P = 0.004$, 0.032) (**b**). **c**, Tumour number, size and load in mice transplanted with indicated bone marrow ($n = 5$, $P = 0.14$, 0.048, 0.046, respectively). **d**–**f**, CPC-APC mice were treated with a cocktail of antibiotics (Abx) for 3 weeks. **d**, Myeloid cells were sorted from tumours and analysed by RT–qPCR, representative of two independent experiments, each including four pooled mice. **e**, IL-17A mRNA expression in normal and tumour tissues from the control and Abx-treated CPC-APC mice ($n = 9$, $P = 0.003$). **f**, Colon sections from mice were stained with phospho-STAT3 antibody, and intensity of staining was quantified ($n = 8$, $P = 0.049$). **g**, WT (*Il23r*$^{+/-}$) or *Il23r*$^{-/-}$ CPC-APC mice were treated with antibiotics for 3.5 months and tumour size and load were determined ($n = 5$, $P = 0.027$ and 0.043). Data represent averages ± s.e.m. *$P < 0.05$. Scale bars, 50μm.

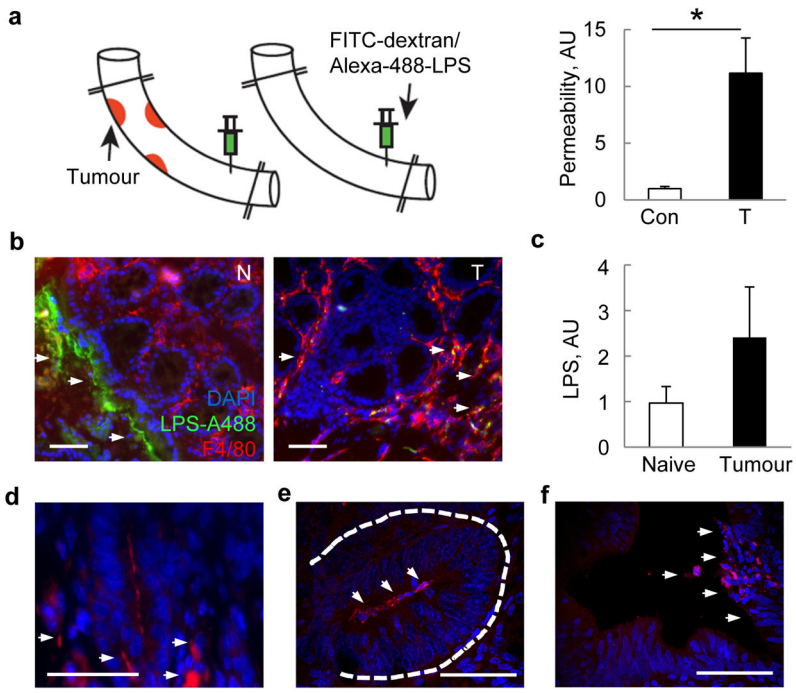

Figure 3. Colorectal tumours exhibit increased permeability to bacteria and their products

a, Colon segments of CPC-APC and control mice were clipped as indicated and their lumens injected with FITC-dextran or Alexa488-LPS. FITC fluorescence was measured in plasma 1 h later ($n = 7$, $P = 0.017$). **b**, Frozen colon sections prepared 30 min after Alexa488-LPS injection were stained with F4/80 antibody and DAPI and examined by fluorescent microscopy. **c**, Endotoxin was measured in portal blood of naive or tumour-bearing CPC-APC mice by *Limulus* bioassay ($n = 9$, $P = 0.066$). **d–f**, Colon sections from CPC-APC mice containing tumours (**d**) and early lesions (aberrant crypt foci) (**e**), and early human adenomas (**f**) were subjected to fluorescent *in situ* hybridization with eubacterial 16S-rRNA-specific Alexa594-labelled probe and stained with DAPI. Signals are indicated by the arrows. Data represent averages ± s.e.m. $*P < 0.05$. Scale bars, 50μm.

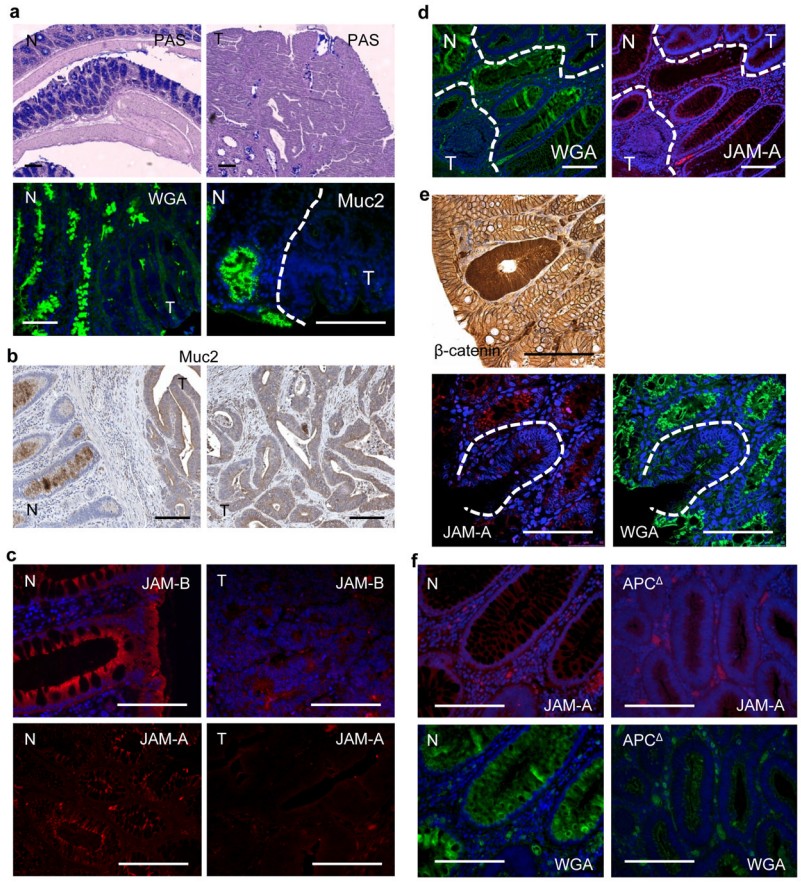

Figure 4. Colorectal tumours show defective mucin production and aberrant expression of junctional proteins

a, Colon sections from CPC-APC mice were stained with periodic acid-Schiff reagent, Oregon488-WGA or mucin 2 antibody. Normal (N) and tumour (T) areas are depicted. **b**, **c**, Sections of normal human colon and adjacent CRC specimens were stained with mucin-2-specific antibody (**b**) or JAM-A or JAM-B antibodies (**c**). **d**, Human adenomas were stained with WGA or JAM-A antibodies. Normal and tumour areas are marked. **e**, Sections of CPC-APC colons were stained with β-catenin antibody and analysed by light microscopy or WGA and JAM-A antibodies and analysed by confocal microscopy. **f**, Colon sections of tamoxifen-injected control or *Cdx2*$^{\text{ERT-Cre}}$ × *Apc*$^{\text{F/F}}$ mice were stained with JAM-A antibody or WGA. Normal (N) and APC-deleted areas are shown. Scale bars, 100μm.